ANALYZING POWER MEASUREMENTS IN MEDIUM-ENERGY PROTON SCATTERING AND THE SPIN-DEPENDENCE OF THE OPTICAL POTENTIAL

P. Schwandt, A.D. Bacher, H.-O. Meyer, W.W. Jacobs and S.E. Vigdor
Indiana University Cyclotron Facility, Bloomington, Indiana 47405

T. Donoghue
The Ohio State University, Columbus, Ohio 43212

The availability of precise differential cross-section measurements and analyzing power data for proton elastic scattering from nuclei over broad ranges of proton energy and target mass is important from two general points of view: (1) for generating a global, phenomenological optical-model description of the proton-nucleus interaction which establishes the systematic energy and target mass dependences of the parametrization and especially of those characteristic quantities such as potential volume integrals and r.m.s. radii which are relatively free from the common ambiguities and correlations inherent in the phenomenolocial model; (2) for assessing the validity of microscopic potential models of the nucleon-nucleus interaction based on the 2-nucleon interaction, either by comparing model predictions with experimental data

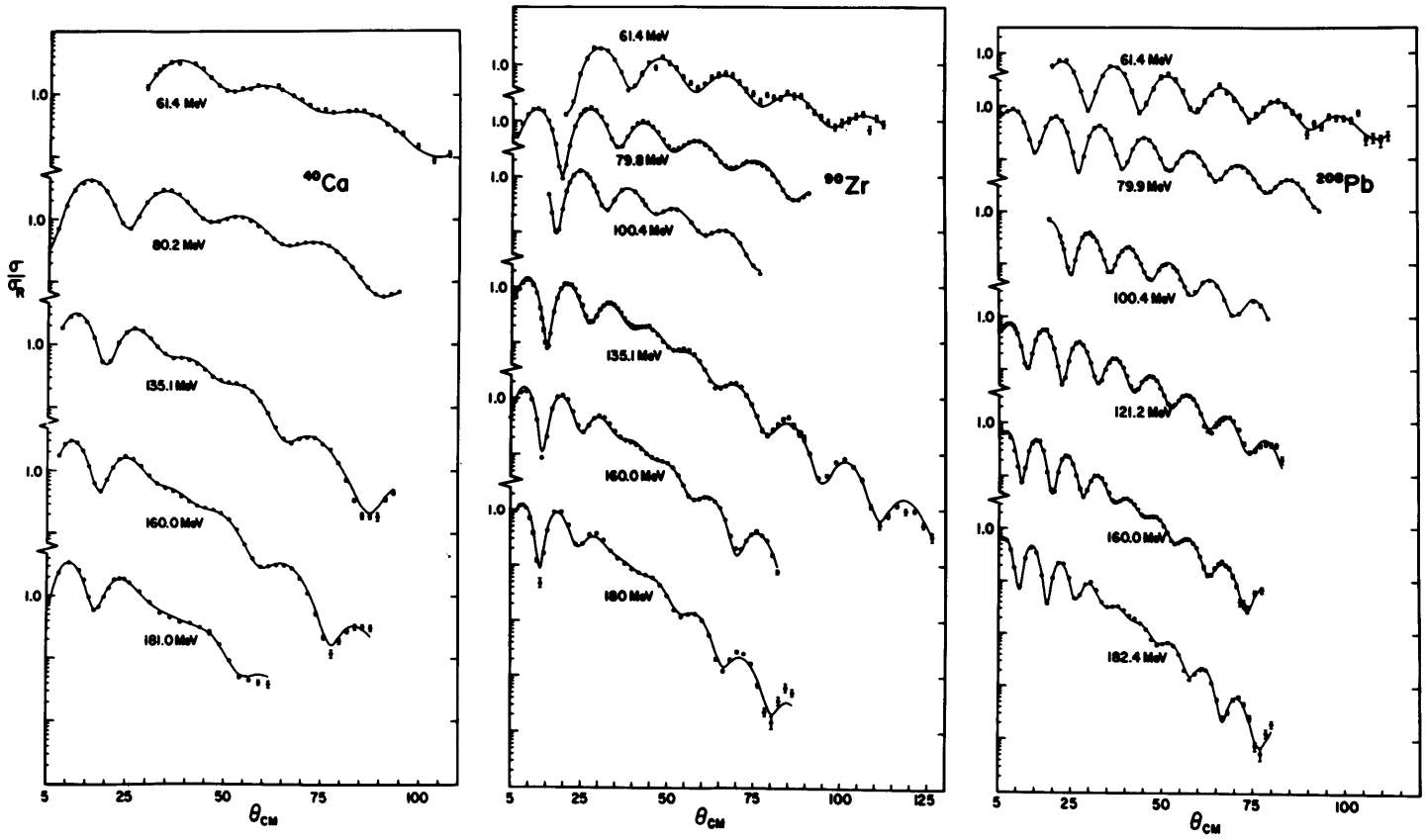

Figure 1. Differential cross section angular distributions in units of ratio-to-Rutherford for proton elastic scattering from ^{40}Zr and ^{208}Pb between 61 and 182 MeV (the 61 MeV data are from Ref. 3, the 100.4 MeV data from Ref. 4, the 181 MeV ^{40}Ca data from Ref. 5).

directly or by comparing salient features of the generalized optical potential (in a local approximation) with those of the phenomenological potential.

The principal features of the central (spin-independent) terms in the empirical optical potential are generally defined by cross-section data with reasonable precision. Until recently, however, reliable determination of the spin-orbit term in the proton optical potential from analyses of elastic scattering data has been possible only at low energies ($E_p \lesssim 60$ MeV) or at the high end of the intermediate-energy range (E_p = 800 and 1000 MeV) because of the scarcity of high-quality analyzing power data at intervening energies. That deficiency is largely removed now by the extensive and precise measurements of both cross sections $\sigma(\theta)$ and analyzing powers $A(\theta)$ from IUCF at energies between 80 and 180 MeV, and by preliminary data from similar measurements underway at TRIUMF at 200 and 400 MeV.

This report presents results of measurements and analyses carried out at IUCF for proton elastic scattering from ^{40}Ca, ^{90}Zr and ^{208}Pb at bombarding energies between 80 and 182 MeV, as well as the analysis of data for ^{208}Pb between 200 and 1000 MeV. The IUCF differential cross section data and their analysis in terms of a phenomenological optical potential have been reported previously[1] and are summarized here in Fig. 1. New analyzing power data for the scattering of polarized proton beams have so far been obtained at IUCF for ^{40}Ca at 181 MeV, for ^{90}Zr at 100, 135 and 160 MeV and for ^{208}Pb at 100 and 182 MeV. Examples of these data are presented in Fig. 2. Additional measurements of this observable are continuing at IUCF. A more detailed description of the experiment can be found in Ref. 2. The available $\sigma(\theta)$ and $A(\theta)$ data for ^{208}Pb between 120 and 1000 MeV proton energy are illustrated in Fig. 3. In this graph σ/σ_R and A are presented as functions of the momentum transfer q to point out, first of all,

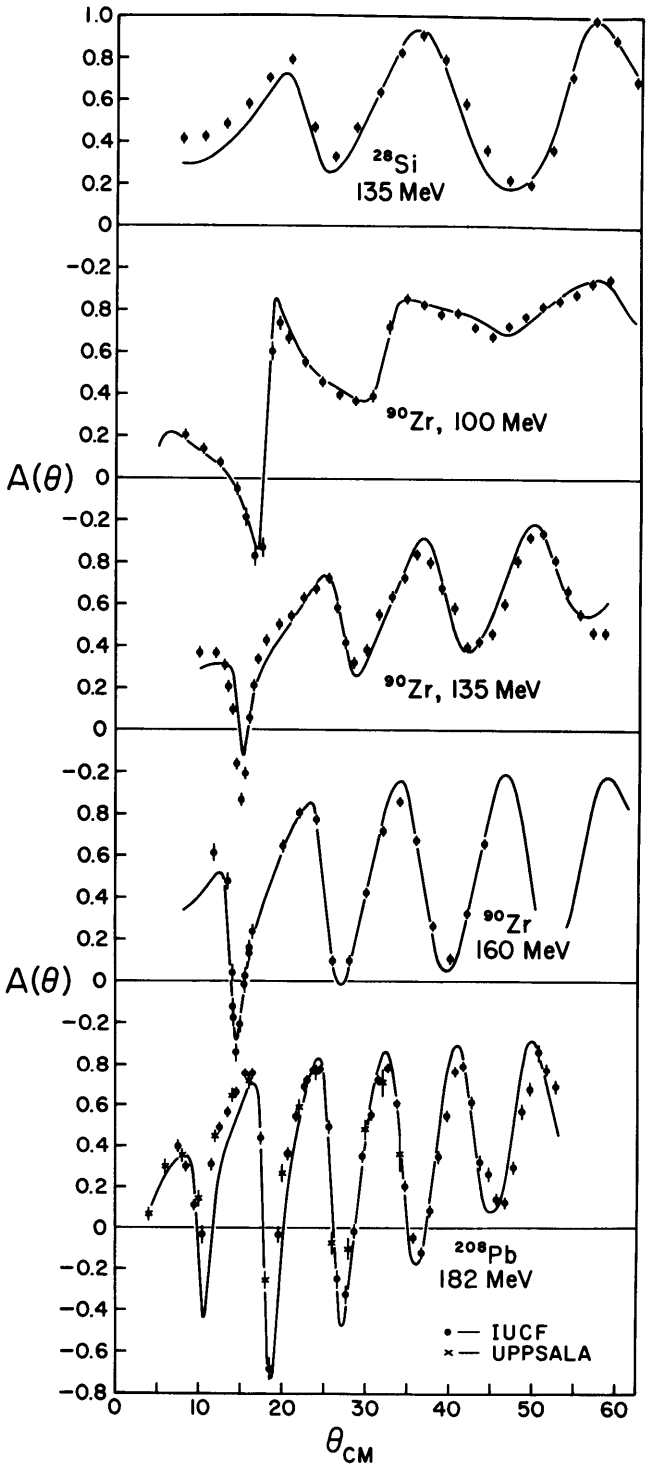

Figure 2. Angular distributions of the analyzing power $A(\theta)$ for $\vec{p}$ scattering from ^{28}Si, ^{90}Zr and ^{208}Pb measured at IUCF (the 182 MeV ^{208}Pb data labelled UPPSALA are from Ref. 6). The curves represent the results of 10-parameter optical-model fits to the $\sigma(\theta)$ and $A(\theta)$ data.

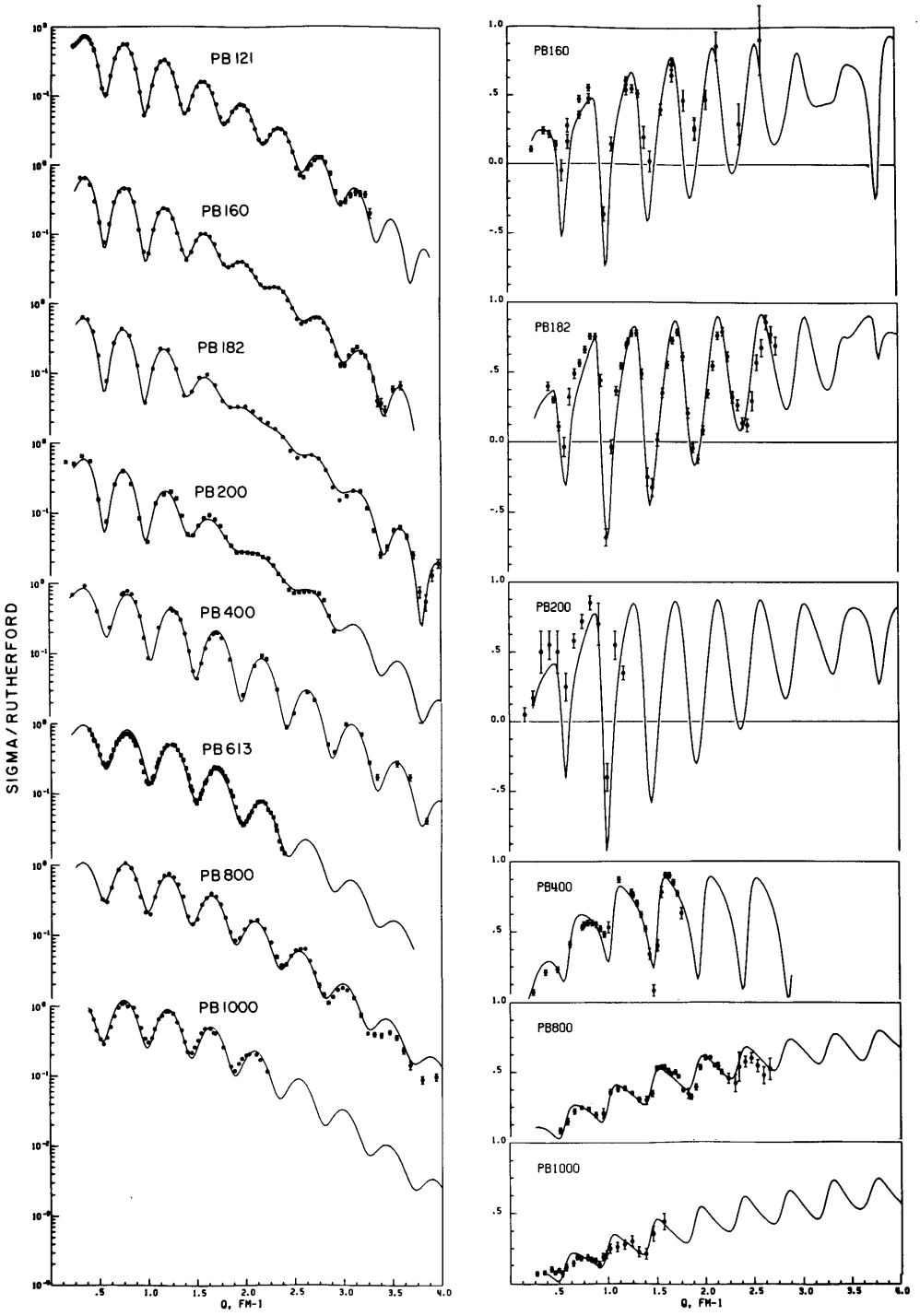

Figure 3. Angular distributions of differential cross sections (normalized to Rutherford scattering) and analyzing powers as functions of momentum transfer for p+^{208}Pb, 121-1000 MeV. The 121-182 MeV data are from IUCF, the 200 and 400 MeV data from TRIUMF, the 613 MeV data[8] from Saclay, the 800 MeV data[9] from LAMPF, and the 1000 MeV data[10] from Gatchina (Leningrad). The curves are optical-model fits.

the loss of a diffraction minimum in σ over the range of q illustrated in going from proton energies below 200 MeV to energies above 200 MeV (a phenomenon associated with the dissappearance of oscillating structure around $q \sim 2$ fm^{-1} at 160-200 MeV and reflected in the optical-model analysis by a gradual 10% decrease in the r.m.s. radius of the real central potential across the transition energy range 150-400 MeV). A second striking feature of the data over this wide energy range is the change in A from a strongly oscillatory function of q (or θ) below 400 MeV to a mildly modulated positive function at 800 MeV and beyond (a feature associated with the transition of the central optical potential from predominantly real to predominantly imaginary

character).

The analysis of these new data, together with selected existing polarization data from other laboratories at energies between 40 and 1000 MeV, firmly establishes the spin dependence of the empirical optical potential for medium-energy proton scattering up to about 200 MeV and provides a first look at the apparently very different energy dependence of the spin-orbit strength beyond 200 MeV. In what follows, the phenomenological results are presented and compared with theory, chiefly in terms of potential volume integrals.

In the phenomenological optical-model analysis of the angular distributions a local, complex, spin-dependent potential of canonical form was employed:

$$U(r) = U_{coul}(r) - Vf_o(r;r_o,a_o) - iWf_w(r;r_w,a_w)$$

$$+ \left(\frac{\hbar}{m_\pi c}\right)^2 [V_{so} + iW_{so}] \frac{1}{r}\frac{d}{dr} f_{so}(r;r_{so},a_{so}) \vec{L}\cdot\vec{\sigma}$$

with Woods-Saxon formfactors $f_k(r;r_k,a_k)$ and 10 free parameters. The analysis was carried out in a semi-relativistic generalization of the conventional (non-relativistic) Schrödinger wave equation, obtained by an appropriate reduction of the Dirac equation for a massive, energetic fermion (mass m_1, kinetic energy T_1, wavenumber k) in a localized potential field U(r) chosen to be the fourth (time-like) component of a Lorentz vector potential and satisfying the conditions $U << m_1$, $\nabla U/U << k$. This reduction yields the Schrödinger-type equation $(\nabla^2-\alpha U)\Psi = \beta T\Psi$ for the large component of the wavefunction where, for non-relativistic motion of the target nucleus, α and β are defined in terms of the total system energy E and projectile, target masses m_1, m_2 by $\alpha = 2m_2(E-m_2)/E$, $\beta = m_2(E-m_2+m_1)/E$. The spin-orbit term appearing in the optical potential U(r) is a purely phenomenological one (the intrinsic S.O. term in the Dirac equation is negligibly small in the above limits assumed to be satisfied by the spin-independent potential).

As is evident from Figs. 1 and 3, the overall quality of fits to the total set of $\sigma(\theta)$ data analyzed is excellent over the whole angular range. The optical-model fits to the analyzing powers $A(\theta)$ illustrated in Figs. 2 and 3 are quite satisfactory overall, although small but significant discrepancies between experiment and calculation can be noted in some cases.

The parameters of the central potential are well defined by the cross section data. A logarithmic energy dependence is found for the strength of the real central potential over the whole energy range, while the corresponding imaginary (absorptive) potential strength is essentially independent of proton energy up to 200 MeV and, as expected, increases rapidly beyond 200 MeV as meson production and nucleon excitation channels open. This is illustrated in Fig. 4 in terms of the normalized potential volume integral, (per unit nucleon mass),

$$J^{cent} \equiv 4\pi\int U^{cent}(r) r^2 dr,$$

which frequently constitutes the meeting point between phenomenology and theory. We find for $60 \lesssim E_p \lesssim 200$ MeV:

$$J_R/A \equiv \mathrm{Re}\, J^{cent}/A \simeq 815 - 120\ \ell n\ E_p \quad (\mathrm{MeV\text{-}fm^3})$$

$$J_I/A \equiv \mathrm{Im}\, J^{cent}/A \simeq 100 \pm 20 \quad (\mathrm{MeV\text{-}fm^3})$$

where E_p is the proton energy in MeV. Beyond 200 MeV, J_R appears to decrease slightly faster with increasing E_p and crosses zero near 600 MeV.

While a markedly increased sensitivity of the differential cross section to spin-orbit effects is found at energies between 100 and 200 MeV (in contrast to lower energies) which results in a reasonable definition of the gross features of the complex S.O. potential and its general trend with proton energy, considerable uncertainties and ambiguities remain in the S.O.

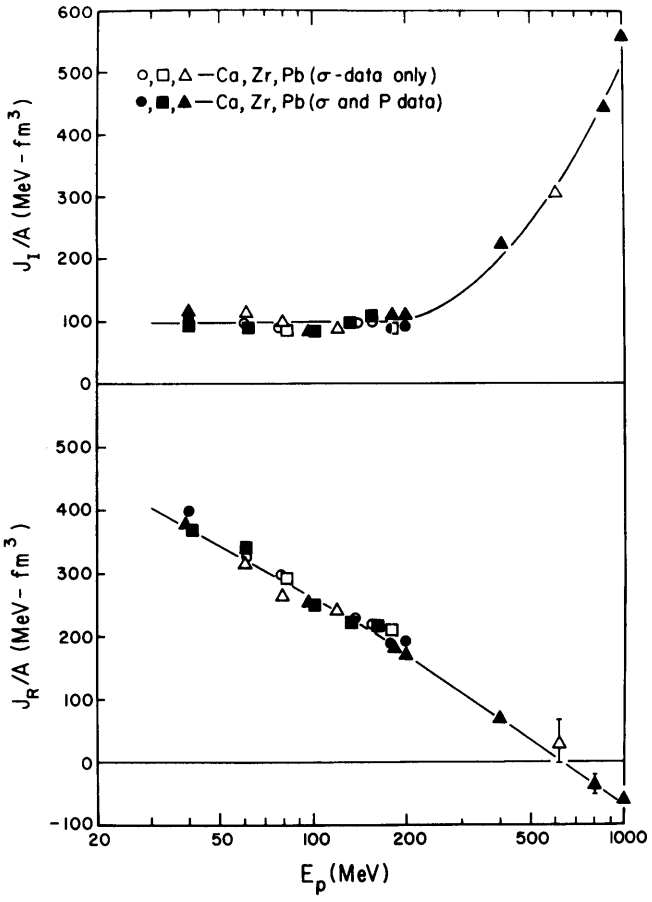

Figure 4. Normalized volume integrals of the imaginary central (top) and real central optical potential (bottom) as functions of proton bombarding energy. Explanation of the symbols is provided in the legend. The curve drawn for J_I is a guide to the eye; the curves drawn for J_R represents best linear fits to the points for the energy regions $E_p \leq 200$ MeV and $E_p > 200$ MeV.

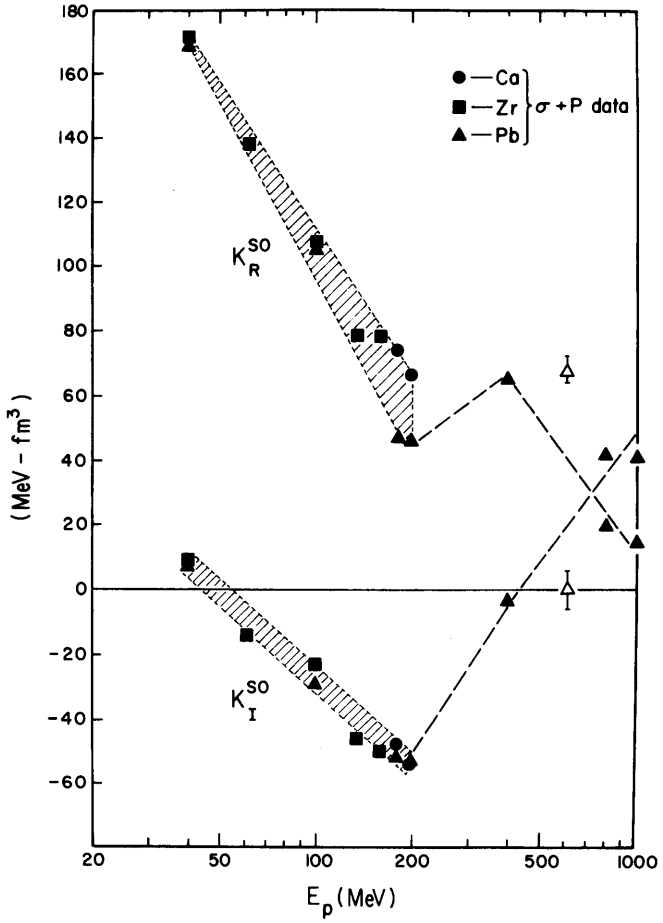

Figure 5. Normalized volume integrals of the real spin-orbit (top) and imaginary spin-orbit optical (bottom) as functions of proton bombarding energy. The solid (open) symbols represent results of analyses of σ + A data (σ data only). The shaded bands define the energy dependence below 200 MeV; the dashed lines suggest the likely behavior beyond 200 MeV.

parametrization based on σ(θ) data alone. A considerably more precise definition of the S.O. potential and its variation with energy is obtained from simultaneous analysis of both σ(θ) and A(θ) data (or polarization data P(θ)), particularly including the new IUCF A(θ) data. These results in terms of the normalized real and imaginary S.O. potential volume integrals, $K^{so}_{R,I} \equiv J^{so}_{R,I}/A^{1/3}$, are shown in Fig. 5 by the solid symbols (open symbols in Figs. 4 and 5 represent results based on analyses of σ(θ) data only). For $E_p \lesssim 200$ MeV we can represent the energy dependence of K^{so}_R and K^{so}_I by the logarithmic relations

$$K^{so}_R \simeq \begin{cases} 430 - 50\ \ell n\ E_p \pm 4\ \text{MeV-fm}^3 & \text{for } ^{40}Ca \\ 470 - 80\ \ell n\ E_p \pm 4\ \text{MeV-fm}^3 & \text{for } ^{208}Pb \end{cases}$$

$$K^{so}_I \simeq 145\text{-}38\ \ell n\ E_p \pm 4\ \text{MeV-fm}^3$$

The real S.O. strength is seen to exhibit significant target-mass dependence between 100 and 200 MeV (encompassed by the shaded region in the upper part of Fig. 5) and decreases substantially with increasing energy up to 200 MeV, while the imaginary S.O. strength is seen to be of opposite sign and increases with energy to a maximum magnitude approaching that of the real S.O. strength near 200 MeV. Beyond 200 MeV, however, the present data indicate a continuing but

non-monotonic decrease of K_R^{so} with E_p, and a reversal of the slope for K_I^{so} which in fact changes sign near 400 MeV. Forthcoming additional measurements at energies between 200 and 500 MeV from TRIUMF are expected to provide a more detailed definition of these trends.

Realistic microscopic calculations of the optical potential in terms of a realistic (i.e., strong) nucleon-nucleon interaction are based on Brueckner-Hartree-Fock (BHF) or multiple-scattering expansions. The BHF approximation is the first term in a low-density expansion of the mass operator in nuclear matter, using a strong interaction v. This yields a non-local as well as energy-dependent optical potential. The most recent and thorough developments of this parameter-free model are due to Jeukenne, Lejeune and Mahaux[11] (JLM) and Brieva and Rook.[12] Of these microscopic formulations of the optical potential, thought valid up to about 200 MeV, only the Brieva and Rook calculation incorporates the complex S.O. part of the optical potential. These authors use an effective, complex transition matrix $t = v + vGt$ and a generalized reference spectrum method to solve the Bethe-Goldstone equation. For comparison with the phenomenological optical model, a complex and energy-dependent local potential is generated with the antisymmetrized folding model and the local density approximation. The Brieva and Rook calculations fail dramatically to reproduce the strong empirical energy dependence of the complex S.O. volume integrals. These calculations underestimate the real part, K_R^{so}, below $\sim$ 80 MeV and overestimate it above $\sim$ 120 MeV; the predicted imaginary part, K_I^{so}, is considerably too small at the higher energies (near 200 MeV) where our choice of identical radial formfactors for V_{so} and W_{so} in fact conforms to the theoretical expectation (the calculations show this assumption to be invalid below $\sim$ 100 MeV).

Beyond 200 MeV, multiple-scattering theory in the impulse approximation (IA), in which the reaction matrix reduces to the transition matrix for free nucleon-nuclear scattering, is expected to provide a simple and useful description. Recent application of this method to medium-energy (150-200 MeV) proton-nucleus scattering by Schwandt and Petrovich[13] has been modestly successful in describing the differential cross sections. These calculations were carried out to lowest order in the multiple-excitation expansion, using a parametrization of the complex, fully anti-symmetrized t-matrix (to incorporate the effect of one-nucleon exchange) due to Love.[14] Unfortunately, the impulse approximation is also found to provide a considerably less satisfactory description of the analyzing power than of the cross sections at 200 and 400 MeV. While reproducing the phenomenological result for K_R^{so} near 200 MeV, the IA fails even worse than the Brieva and Rook calculation for K_I^{so}. We are presently investigating to what extent the approximate treatment of exchange and neglect of higher-order effects (e.g., Pauli principle effects) in the impulse approximation calculation influence this discrepancy. At 400 MeV, the first-order IA calculations reproduce the empirical values of the S.O. volume integrals (particularly the near-zero value of K_I^{so}) fairly well but nonetheless provides an unsatisfactory description of the analyzing power angular distribution. This is in contrast to the situation at 800 MeV where the IA, even in first order, gives an accurate account of both $\sigma(\theta)$ and $A(\theta)$, albeit with some semi-empirical adjustment of parameters for the spin-dependent component of the 2-nucleon t-matrix dictated by the lack of reliable 2-nucleon phase shifts at that energy.

The principal conclusion to be drawn from the above comparison of microscopic model calculations with experimental data or empirical optical-model results is that at present no satisfactory theoretical description of the spin-dependence of the generalized proton optical potentials exists at energies below 400 MeV.

1) P. Schwandt et al., IUCF Techn. and Scient. Report 1977, p. 79; A. Nadasen et al., submitted to Phys. Rev. C.

2) P. Schwandt et al., IUCF Techn. and Scient. Report 1978, p. 24.

3) C.B. Fulmer et al., Phys. Rev. 181, 1565 (1969).

4) K. Kwiatkowski and N.S. Wall, Nucl. Phys. A301, 349 (1978).

5) A. Johansson et al., Arkiv für Fysik 19, 541 (1961).

6) W.T.H. van Oers et al., Phys. Rev. C10, 307 (1974).

7) Preliminary data, courtesy of D. Hutcheon (TRIUMF).

8) G. Bruge, CEN Saclay Intern. Report DPh-N/ME/78-1.

9) G.S. Blanpied et al., Phys. Rev. C18, 1436 (1978).

10) G.D. Alkhazov et al., Leningrad preprint No. 26 (1977) p. 715.

11) J.P. Jeukenne, A. Lejeune and C. Mahaux, Phys. Rev. C16, 80 (1977).

12) F.A. Brieva and J.R. Rook, Nucl. Phys. A291, 299 and 317 (1977); ibid., Nucl. Phys. A297, 206 (1978); ibid., Nucl. Phys. A307, 493 (1978).

13) P. Schwandt and F. Petrovich, IUCF Techn. and Scient. Report 1978, p. 27.

14) W.G. Love et al., Phys. Lett. 73B, 277 (1978).

DEUTERON ELASTIC SCATTERING CROSS-SECTION AND VECTOR ANALYZING POWER MEASUREMENTS FOR ^{58}Ni AND ^{208}Pb AT 79.5 MeV

C.C. Foster, J.C. Collins, D.L. Friesel, W.W. Jacobs, W.P. Jones, S. Kailas, M. Kaitchuck
P. Schwandt, and E.J. Stephenson
Indiana University Cyclotron Facility, Bloomington, Indiana 47405

W.W. Daehnick
University of Pittsburgh, Pittsburgh, Pennsylvania 15260

Differential cross-section and vector analyzing power angular distributions have been measured for elastic scattering of 79.5 MeV deuterons from ^{58}Ni, $8^{\circ} \leq \theta_{Lab} \leq 60^{\circ}$, and from ^{208}Pb, $14^{\circ} < \theta_{Lab} \leq 53^{\circ}$. The QDDM spectrograph was used in a one-arm experiment with the IUCF polarized beam. The beam polarization was obtained from $\vec{d} + \alpha$ elastic scattering at 7.1 MeV in the intermachine beam line. A two arm polarimeter with a helium gas target was used to determine the vector polarization of the spin-up and spin-down beam. Unpolarized beam measurements were made to obtain and minimize the unwanted tensor component of the beam polarization. The analyzing power data for $\vec{d} + \alpha$ elastic scattering of W. Grüebler et al.[1] were used in calculating beam polarization.

Figure 1 shows cross section and vector analyzing power angular distributions for ^{58}Ni$(\vec{d},d)$, and Fig. 2 shows similar measurements for ^{208}Pb$(\vec{d},d)$. These measurements have been included in the recent global optical model analysis of elastic deuteron scattering by W. Daehnick et al.[2] Final values for the differential cross sections for these targets are tabulated in the appendix of this report. An as yet unresolved discrepancy of about 27% in the analyzing power normalization between the two available in-house measurements on ^{58}Ni means the analyzing power results for ^{58}Ni and ^{208}Pb must presently be considered preliminary.

Noteworthy features of these data are the smooth fall-off of the differential cross section at large angles and the indication in the ^{58}Ni data of a corresponding rise of the vector analyzing power to a large positive value at back angles. The